

Dispersion relation reconstruction for 2D Photonic Crystals based on polynomial interpolation

Yueqi Wang*, Guanglian Li† and Richard Craster‡

Abstract

Dispersion relation reflects the dependence of wave frequency on its wave vector when the wave passes through certain material. It demonstrates the properties of this material and thus it is critical. However, dispersion relation reconstruction is very time consuming and expensive. To address this bottleneck, we propose in this paper an efficient dispersion relation reconstruction scheme based on global polynomial interpolation for the approximation of 2D photonic band functions. Our method relies on the fact that the band functions are piecewise analytic with respect to the wave vector in the first Brillouin zone. We utilize suitable sampling points in the first Brillouin zone at which we solve the eigenvalue problem involved in the band function calculation, and then employ Lagrange interpolation to approximate the band functions on the whole first Brillouin zone. Numerical results show that our proposed methods can significantly improve the computational efficiency.

1 Introduction

Photonic Crystals (PhCs) are periodic dielectric materials with size of their period comparable to the wavelength [17]. The propagation of electromagnetic waves inside such materials depends heavily on their frequencies. Furthermore, electromagnetic waves within a certain frequency range cannot propagate in certain PhCs. This forbidden frequency range is the so-called band gap, which motivates many important applications, including optical transistors, photonic fibers and low-loss optical mirrors [35, 27, 24]. In this paper, we focus on 2D PhCs which are periodic in the xy plane and homogeneous along the z axis with high-contrast dielectric columns or holes spaced in dielectric materials.

To fully understand PhCs, research interest falls on the propagating frequency as well as the band gap. The periodicity of PhCs allows using the Bloch's theory so that the original Helmholtz eigenvalue problem on the whole space is transformed into a family of Helmholtz eigenvalue problems defined on the unit cell parameterized by the wave vector \mathbf{k} varying in the irreducible Brillouin zone (IBZ) [23]. The frequency ω_n which is a scaling of the n th largest eigenvalue, regarded as a function of the wave vector \mathbf{k} is the so-called the n th band function for all $n \in \mathbb{N}^+$. The band gap is the distance between two adjacent band functions. Consequently,

*Department of Mathematics, The University of Hong Kong, Pokfulam Road, Hong Kong. Email: u3007895@connect.hku.hk

†Department of Mathematics, The University of Hong Kong, Pokfulam Road, Hong Kong. Email: lotusli@maths.hku.hk

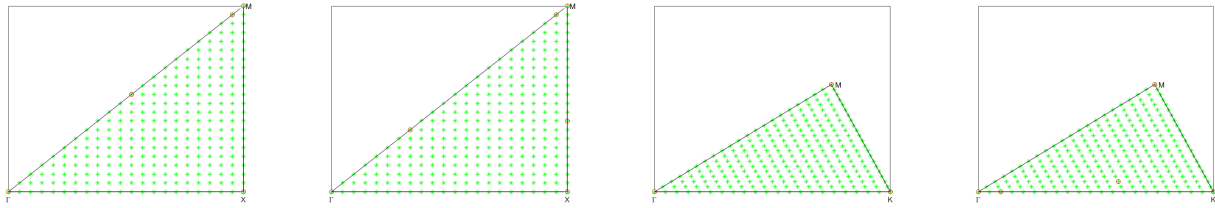
‡Department of Mathematics, Imperial College London, London SW7 2AZ, UK. Email: r.craster@imperial.ac.uk

the calculation of the n th band function $\omega_n(\mathbf{k})$ involves solving infinite number of the Helmholtz eigenvalue problems defined on the unit cell parameterized by the wave vector \mathbf{k} varying in the IBZ, which have high-contrast, piecewise constant coefficients. To reduce this computational cost, a natural approach is to decrease the number of parameters \mathbf{k} by limiting them to the edges of the IBZ. A practical approach is to discretize the edges of the IBZ uniformly to generate the parameters. Although there is no rigorous theoretical foundation, this approach demonstrates its accuracy for many numerical tests on 2D PhCs. To further reduce the number of parameters, several sampling algorithms have been proposed. In specific, Hussein introduced the model order reduction method to band gap calculation and proposed to use the high symmetry points and the intermediate points centrally intersecting the straight lines joining these high symmetry points as the sampling points [14]. Klindworth proposed to use Taylor expansion to approximate the reordered band functions based on the fact that band functions can be reordered so that they are analytic functions of \mathbf{k} and an adaptive step size controlling was proposed to determine the sampling points [22]. In addition, some improvements to these methods have also been proposed in recent years [30, 18, 19].

1.1 Motivation for sampling inside of the IBZ

However, recently the question of whether the edges of the IBZ are sufficient to characterize the band gap has received intensive interest. Figure 1 illustrates the extrema of the first six band functions of two 2D PhCs as depicted in Figures 4 and 5. One can observe that they are not always detected on the edges of the IBZ. In fact, Figure 1(d) depicts an extremum inside the IBZ which is the maximum value of the sixth band function. In Table 1 we present this maximum value and compare it with the maximum value of this case obtained only using the edges of the IBZ, which demonstrates the importance of the interior information. Furthermore, some work has shown counterexamples that highlight the dangers of just using IBZ edges [11, 25, 7]. Thus, it is urgent to develop an accurate and efficient sampling algorithm on the whole IBZ.

Nevertheless, to the best of our knowledge, there have been no trials in designing such kind of sampling algorithms. To fill this vacancy, we propose in this paper the use of several efficient sampling algorithms that can be combined with Lagrange interpolants to approximate band functions in the whole IBZ. The core spirit of our method is based upon the fact that band functions are piecewise analytic and all the singular points appear on branch points and origin only. The piecewise analyticity was first proved by Wilcox for the case of 2D Schrödinger equation [34], and it was further applied to PhCs [1] by Kuchment for the general elliptic operator [23]. We initiate the study of band function approximation by first summarizing the properties of band functions in details. Then we discuss several feasible ways of selecting sampling points, and estimate the upper bound on the interpolation error of using them to approximate band functions. This work is built upon several well-developed sampling algorithms, which are wildly used in function approximation [2, 32, 4, 28, 6].



(a) TM mode square lattice (b) TE mode square lattice (c) TM mode hexagonal lattice (d) TE mode hexagonal lattice

Figure 1: Extrema exist at points marked with red circles, and green points are used to measure the extrema.

IBZ			IBZ edges	
Band number	\mathbf{k}	Extrema	\mathbf{k}	Extrema
6	(0.719762, 0.049867)	Maxi = 1.071796	(0.690971, 0)	Maxi = 1.069602

Table 1: TE mode hexagonal lattice: band function's extrema obtained using IBZ and IBZ edges.

1.2 Main contributions

Our main contributions are twofold. On the one hand, we analyze and summarize key regularity properties of band functions, cf. Theorems 3.2 and 3.6: First, band functions are piecewise analytic functions; Second, singularities occur on branch points and original point only. These two results are proved by showing that the graphs of all the band functions to the 2nd power $\{\omega_n^2(\mathbf{k})\}_{n=1}^\infty$, which are indeed the Bloch variety defined in (3.1), are zeros of a real analytic function in \mathbb{R}^3 , and the locations of singular points in these graphs are confirmed via implicit mapping theorem; Third, we give the formula for calculating the first derivative of band functions at non-singularities, and thus point out that the first derivative of band functions may be discontinuous at branch points where the dimension of $\ker(\mathcal{L}_{\mathbf{k}} - \lambda(\mathbf{k}))$ is greater than one. This formula further shows that band functions are Lipschitz continuous functions.

On the other hand, our proposed method approximates band functions in the whole IBZ, and we can incorporate it into many other numerical methods, e.g., adaptive FEM [9], hp FEM [31], to calculate band functions with high accuracy and efficiency. Moreover, our method can be utilized without rearranging band functions that is crucial for Taylor expansion based method as developed in [22]. However, the aforementioned approach can only approximate the whole band functions simultaneously instead of the first few band functions, which are the interest of many practical applications.

This paper is organized as follows. In Sections 2, we describe the Maxwell eigenvalue problem involved in band structure calculation and elaborate on the derivation of the parameterized eigenvalue problem through Bolch's theorem as well as the two modes in two-dimensional PhCs. Section 3 is concerned with the main regularity of the band functions, based upon which we introduce the numerical schemes to reconstruct these band functions in Section 4. Extensive numerical experiments are illustrated in Section 5 to support our theoretical findings. Finally, we present in Section 6 conclusions and future work. To improve the readability, some auxiliary results about the band functions are provided in Section A. We believe that the present paper

is the first contribution to the topic of the band structure approximation in the whole IBZ for 2D PhCs based on polynomials.

2 Preliminaries

To study the propagation of light in Photonic Crystals, we begin with the macroscopic Maxwell equations. In SI convention, the Maxwell equations are composed of the following four equations [16]:

$$\begin{aligned}\nabla \times \mathbf{E} + \frac{\partial \mathbf{B}}{\partial t} &= 0, \\ \nabla \times \mathbf{H} - \frac{\partial \mathbf{D}}{\partial t} &= \mathbf{J}, \\ \nabla \cdot \mathbf{D} &= \rho, \\ \nabla \cdot \mathbf{B} &= 0,\end{aligned}$$

where \mathbf{E} is the electric field, \mathbf{H} is the magnetic field, \mathbf{D} is the electric displacement field, \mathbf{B} is the magnetic induction field, \mathbf{J} is the free current density, ρ is the free charge density. Assuming there are no sources of light, we can set $\mathbf{J} = \mathbf{0}$ and $\rho = 0$.

It is conventional to use the so-called constitutive relations to describe how \mathbf{D} and \mathbf{B} depend on \mathbf{E} and \mathbf{H} . Strictly speaking, the constitutive relations are nonlinear. However, for most of the dielectric materials, we assume the field strengths are sufficiently weak and the materials are isotropic and nondispersive media, then it is reasonable to use the following linear approximations:

$$\begin{aligned}\mathbf{D} &= \epsilon_0 \epsilon \mathbf{E}, \\ \mathbf{B} &= \mu_0 \mu \mathbf{H},\end{aligned}$$

where ϵ_0 is the vacuum permittivity, ϵ is the relative permittivity, μ_0 is the vacuum permeability, and μ is the relative magnetic permeability. Note that here both ϵ and μ are scalar functions that map points in \mathbb{R}^3 to \mathbb{R} and $\epsilon, \mu \in L^\infty(\mathbb{R}^3)$. In most Photonic Crystals, it is assumed that the materials are nonmagnetic, i.e. $\mu \equiv 1$.

After introducing all of the above assumptions, the Maxwell equations can be formulated as

$$\nabla \times \mathbf{E} + \mu_0 \frac{\partial \mathbf{H}}{\partial t} = 0, \tag{2.1a}$$

$$\nabla \times \mathbf{H} - \epsilon_0 \epsilon \frac{\partial \mathbf{E}}{\partial t} = 0, \tag{2.1b}$$

$$\nabla \cdot (\epsilon \mathbf{E}) = 0, \tag{2.1c}$$

$$\nabla \cdot \mathbf{H} = 0. \tag{2.1d}$$

Here both \mathbf{E} and \mathbf{H} are functions of time and space, i.e. $\mathbf{E} = \mathbf{E}(\mathbf{x}, t)$, $\mathbf{H} = \mathbf{H}(\mathbf{x}, t)$, while the coefficients of these partial differential equations are time-independent. Thus, we can use the Fourier transformation in time domain to decompose the functions \mathbf{E} and \mathbf{H} depending on space and time into functions depending on spatial frequency, i.e.

$$\begin{aligned}\mathbf{E}(\mathbf{x}) &:= \mathbf{E}(\mathbf{x}, \omega) = \int_{\mathbb{R}} \mathbf{E}(\mathbf{x}, t) e^{i\omega t} dt, \\ \mathbf{H}(\mathbf{x}) &:= \mathbf{H}(\mathbf{x}, \omega) = \int_{\mathbb{R}} \mathbf{H}(\mathbf{x}, t) e^{i\omega t} dt.\end{aligned}$$

According to

$$\int_{\mathbb{R}} \frac{\partial \mathbf{u}}{\partial t}(\mathbf{x}, t) e^{i\omega t} dt = -i\omega \int_{\mathbb{R}} \mathbf{u}(\mathbf{x}, t) e^{i\omega t} dt,$$

and further applying the Fourier transform operator to equations (2.1a)-(2.1d), we get the time harmonic Maxwell equations:

$$\nabla \times \mathbf{E}(\mathbf{x}) - i\omega\mu_0\mathbf{H}(\mathbf{x}) = 0, \quad (2.2a)$$

$$\nabla \times \mathbf{H}(\mathbf{x}) + i\omega\epsilon_0\epsilon(\mathbf{x})\mathbf{E}(\mathbf{x}) = 0, \quad (2.2b)$$

$$\nabla \cdot (\epsilon(\mathbf{x})\mathbf{E}(\mathbf{x})) = 0, \quad (2.2c)$$

$$\nabla \cdot \mathbf{H}(\mathbf{x}) = 0. \quad (2.2d)$$

Remark 2.1. *Since the Fourier transformation forms complex-valued fields, we should remember to take the real part of the above equations to obtain the physical fields.*

Now applying the curl operator to (2.2a) and using (2.2b), we obtain

$$\nabla \times (\nabla \times \mathbf{E}(\mathbf{x})) - \left(\frac{\omega}{c}\right)^2 \epsilon(\mathbf{x})\mathbf{E}(\mathbf{x}) = 0, \quad (2.3)$$

where $\epsilon_0\mu_0 = c^{-2}$. Similarly, applying the curl operator to (2.2b) and using (2.2a), we obtain

$$\nabla \times \left(\left(\frac{1}{\epsilon(\mathbf{x})} \right) \nabla \times \mathbf{H}(\mathbf{x}) \right) - \left(\frac{\omega}{c} \right)^2 \mathbf{H}(\mathbf{x}) = 0. \quad (2.4)$$

For a given frequency ω , we can find the existence of the spatial pattern $\mathbf{E}(\mathbf{x})$ and $\mathbf{H}(\mathbf{x})$ through the above equations (2.3) and (2.4). In fact, we only need to consider one of the above equations, since we can derive from (2.2a) and (2.2b) that

$$\mathbf{H}(\mathbf{x}) = -\frac{i}{\omega\mu_0} \nabla \times \mathbf{E}(\mathbf{x}), \quad (2.5a)$$

$$\mathbf{E}(\mathbf{x}) = \frac{i}{\omega\epsilon_0\epsilon(\mathbf{x})} \nabla \times \mathbf{H}(\mathbf{x}). \quad (2.5b)$$

Remark 2.2. *The two divergence equations (2.2c) and (2.2d) are implicitly satisfied, which can easily be seen by applying the divergence operator to equations (2.2a) and (2.2b), and considering the fact that $\omega > 0$. Hence, now we only focus on the other two of the time harmonic Maxwell equations as long as we drop those “spurious modes” existing at $\omega = 0$.*

To summarize, the eigenvalue problems (2.3) and (2.4) are two crucial parts of studying the propagation of electromagnetic waves in PhCs and our aim is to find the eigenpairs (ω, \mathbf{E}) and (ω, \mathbf{H}) satisfying these two equations, respectively.

2.1 Modes in two-dimensional Photonic Crystals

In 2D case, the permittivity ϵ is invariant in the direction of the holes or rods, the z -direction. Hence, the permittivity ϵ satisfies $\epsilon(\mathbf{x}) = \epsilon(x, y, 0)$, for all $\mathbf{x} = (x, y, z) \in \mathbb{R}^3$. So we can also restrict our electric field and magnetic field to the xy plane, i.e.

$$\mathbf{E}(\mathbf{x}) = \mathbf{E}(x, y, 0) = (E_1(x, y, 0), E_2(x, y, 0), E_3(x, y, 0)),$$

$$\mathbf{H}(\mathbf{x}) = \mathbf{H}(x, y, 0) = (H_1(x, y, 0), H_2(x, y, 0), H_3(x, y, 0)),$$

for all $\mathbf{x} = (x, y, z) \in \mathbb{R}^3$. Then a straightforward calculation leads to

$$\nabla \times \mathbf{E} = \left(\frac{\partial E_3}{\partial y} \right) \mathbf{i} + \left(-\frac{\partial E_3}{\partial x} \right) \mathbf{j} + \left(\frac{\partial E_2}{\partial x} - \frac{\partial E_1}{\partial y} \right) \mathbf{k}, \quad (2.6)$$

$$\nabla \times (\nabla \times \mathbf{E}) = \left(\frac{\partial^2 E_2}{\partial y \partial x} - \frac{\partial^2 E_1}{\partial y^2} \right) \mathbf{i} + \left(-\frac{\partial^2 E_2}{\partial x^2} + \frac{\partial^2 E_1}{\partial x \partial y} \right) \mathbf{j} + \left(-\frac{\partial^2 E_3}{\partial x^2} - \frac{\partial^2 E_3}{\partial y^2} \right) \mathbf{k}, \quad (2.7)$$

$$\nabla \times \mathbf{H} = \left(\frac{\partial H_3}{\partial y} \right) \mathbf{i} + \left(-\frac{\partial H_3}{\partial x} \right) \mathbf{j} + \left(\frac{\partial H_2}{\partial x} - \frac{\partial H_1}{\partial y} \right) \mathbf{k}, \quad (2.8)$$

$$\begin{aligned} \nabla \times \left(\frac{1}{\epsilon(\mathbf{x})} \nabla \times \mathbf{H} \right) &= \left(\frac{\partial}{\partial y} \frac{1}{\epsilon(\mathbf{x})} \frac{\partial H_2}{\partial x} - \frac{\partial}{\partial y} \frac{1}{\epsilon(\mathbf{x})} \frac{\partial H_1}{\partial y} \right) \mathbf{i} + \left(-\frac{\partial}{\partial x} \frac{1}{\epsilon(\mathbf{x})} \frac{\partial H_2}{\partial x} + \frac{\partial}{\partial x} \frac{1}{\epsilon(\mathbf{x})} \frac{\partial H_1}{\partial y} \right) \mathbf{j} + \\ &\quad \left(-\frac{\partial}{\partial x} \frac{1}{\epsilon(\mathbf{x})} \frac{\partial H_3}{\partial x} - \frac{\partial}{\partial y} \frac{1}{\epsilon(\mathbf{x})} \frac{\partial H_3}{\partial y} \right) \mathbf{k}. \end{aligned} \quad (2.9)$$

Plugging (2.7) into (2.3), we obtain

$$-\Delta E_3(\mathbf{x}) - \left(\frac{\omega}{c} \right)^2 \epsilon(\mathbf{x}) E_3(\mathbf{x}) = 0, \quad \text{in } \mathbb{R}^2.$$

Combining with (2.6), (2.5a) implies

$$\begin{aligned} H_1(\mathbf{x}) &= -\frac{i}{\omega \mu_0} \frac{\partial}{\partial y} E_3(\mathbf{x}), \\ H_2(\mathbf{x}) &= \frac{i}{\omega \mu_0} \frac{\partial}{\partial x} E_3(\mathbf{x}). \end{aligned}$$

Analogously, we derive

$$-\nabla \cdot \frac{1}{\epsilon(\mathbf{x})} \nabla H_3(\mathbf{x}) - \left(\frac{\omega}{c} \right)^2 H_3(\mathbf{x}) = 0, \quad \text{in } \mathbb{R}^2.$$

Following equation (2.8) and (2.5b), we get

$$\begin{aligned} E_1(\mathbf{x}) &= \frac{i}{\omega \epsilon_0 \epsilon(\mathbf{x})} \frac{\partial}{\partial y} H_3(\mathbf{x}), \\ E_2(\mathbf{x}) &= -\frac{i}{\omega \epsilon_0 \epsilon(\mathbf{x})} \frac{\partial}{\partial x} H_3(\mathbf{x}). \end{aligned}$$

The above derivation yields two scalar eigenvalue problems and we also deduce that the components of the electric field and magnetic field are not independent. Indeed, H_1, H_2 are related to E_3 , and E_1, E_2 are related to H_3 . Thus, we can classify the electromagnetic waves in terms of whether E_3 or H_3 equals to zero. which is often referred to as TE mode and TM mode respectively. In other words, in TE mode, the magnetic field is directed along the z axis and the electric field is normal to this axis, while TM mode consists of electric field parallel and magnetic field normal to the z axis.

To conclude, the eigenvalue problems in 2D PhCs reduce to

$$-\Delta E(\mathbf{x}) - \left(\frac{\omega}{c} \right)^2 \epsilon(\mathbf{x}) E(\mathbf{x}) = 0, \quad \text{in } \mathbb{R}^2 \quad \text{(TM mode)}, \quad (2.10)$$

$$-\nabla \cdot \frac{1}{\epsilon(\mathbf{x})} \nabla H(\mathbf{x}) - \left(\frac{\omega}{c} \right)^2 H(\mathbf{x}) = 0, \quad \text{in } \mathbb{R}^2 \quad \text{(TE mode)}. \quad (2.11)$$

2.2 Bloch's theorem

Bloch's theorem states that in periodic crystals, wave functions take the form of a plane wave modulated by a periodic function. Mathematically, they can be written as

$$\Psi(\mathbf{x}) = e^{i\mathbf{k}\cdot\mathbf{x}}u(\mathbf{x}),$$

where Ψ is the wave function, $u(\mathbf{x})$ is a periodic function with the same periodicity as the crystal lattice, \mathbf{k} is the wave vector. Functions of this form are known as Bloch functions or Bloch states.

Proposition 2.1. *The periodicity condition of $u(\mathbf{x})$ implies that each Bloch state can be determined by its values within the unit cell Ω spanned by the primitive lattice vectors. So it is sufficient to study only in the unit cell Ω .*

Proposition 2.2. *In 2D case, $e^{i(\mathbf{k}+\mathbf{n}\cdot\mathbf{b})\cdot\mathbf{x}} = e^{i\mathbf{k}\cdot\mathbf{x}}$, where $\mathbf{n} = (n_1, n_2) \in (\mathbb{Z}^+)^2$, $\mathbf{b} = (\mathbf{b}_1, \mathbf{b}_2)$, and each \mathbf{b}_i is the reciprocal lattice vector with the property $\mathbf{b}_i \cdot \mathbf{a}_j = 2\pi\delta_{ij}$ for all primitive lattice vectors \mathbf{a}_j . Thus, the wave vector can be restricted into the unit reciprocal lattice \mathcal{B} , which is the so-called first Brillouin zone. In addition, note that in some cases, further utilization of symmetry can even restrict \mathbf{k} to the irreducible Brillouin zone.*

By Bloch's theorem, we have $E(\mathbf{x}) = e^{i\mathbf{k}\cdot\mathbf{x}}u_1(\mathbf{x})$, $H(\mathbf{x}) = e^{i\mathbf{k}\cdot\mathbf{x}}u_2(\mathbf{x})$, and hence the eigenvalue problems (2.10) and (2.11) reduce to

$$-(\nabla + i\mathbf{k}) \cdot ((\nabla + i\mathbf{k})u_1(\mathbf{x})) - \left(\frac{\omega}{c}\right)^2 \epsilon(\mathbf{x})u_1(\mathbf{x}) = 0, \text{ in } \Omega \quad (\text{TM mode}), \quad (2.12a)$$

$$-(\nabla + i\mathbf{k}) \cdot \left(\frac{1}{\epsilon(\mathbf{x})}(\nabla + i\mathbf{k})u_2(\mathbf{x})\right) - \left(\frac{\omega}{c}\right)^2 u_2(\mathbf{x}) = 0, \text{ in } \Omega \quad (\text{TE mode}), \quad (2.12b)$$

where \mathbf{k} varies in the first Brillouin zone, and $u_i(\mathbf{x})$ satisfies the periodic boundary conditions $u_i(\mathbf{x}) = u_i(\mathbf{x} + \mathbf{a}_j)$ with \mathbf{a}_j being the primitive lattice vector for $i, j = 1, 2$.

Now we consider both modes simultaneously by

$$-(\nabla + i\mathbf{k}) \cdot \alpha(\mathbf{x})(\nabla + i\mathbf{k})u(\mathbf{x}) - \lambda\beta(\mathbf{x})u(\mathbf{x}) = 0, \quad \text{in } \Omega, \quad (2.13)$$

with $\mathbf{k} \in \mathcal{B}$ and $\lambda = \left(\frac{\omega}{c}\right)^2$. In the TM mode, U describes the electric field E in z -direction and the coefficients $\alpha(\mathbf{x})$ and $\beta(\mathbf{x})$ are

$$\alpha(\mathbf{x}) := 1, \quad \beta(\mathbf{x}) := \epsilon(\mathbf{x}).$$

Similarly, in the TE mode, U describes the magnetic field H in z -direction and the coefficients $\alpha(\mathbf{x})$ and $\beta(\mathbf{x})$ are

$$\alpha(\mathbf{x}) := \frac{1}{\epsilon(\mathbf{x})}, \quad \beta(\mathbf{x}) := 1.$$

3 Regularity of band functions and eigenfunctions

To further analyze the properties of band functions, we first define some function spaces. Let $L^2(\Omega)$ denote the space of square integrable functions equipped with the weighted norm

$$\|f\|^2 = \int_{\Omega} |f(\mathbf{x})|^2 \beta(\mathbf{x}) d\mathbf{x}.$$

Let the Sobolev space $H^1(\Omega)$ be the subspace of $L^2(\Omega)$ whose weak gradient is also square integrable with the usual H^1 -norm. Denote $H_\pi^1(\Omega)$ by the subspace of $H^1(\Omega)$ whose functions satisfy periodic conditions on $\partial\Omega$. Moreover, let

$$H_\pi^1(\Omega, \Delta, \alpha) := \{v \in H_\pi^1(\Omega) : \Delta v \in L^2(\Omega), \alpha \partial_{\mathbf{n}_L} v|_L = -\alpha \partial_{\mathbf{n}_R} v|_R \text{ and } \alpha \partial_{\mathbf{n}_T} u|_T = -\alpha \partial_{\mathbf{n}_B} u|_B\}$$

with $\partial_{\mathbf{n}_L}, \partial_{\mathbf{n}_R}, \partial_{\mathbf{n}_B}, \partial_{\mathbf{n}_T}$ denoting the outward normal derivatives on the left, right, bottom and top boundaries of Ω , respectively.

The Bloch's theorem expand the original operator $\mathcal{L} := -\frac{1}{\beta(\mathbf{x})} \nabla \cdot \alpha(\mathbf{x}) \nabla$ defined on Sobolev space $H^2(\mathbb{R}^2)$ into a new set of operators $\mathcal{L}_{\mathbf{k}} := -\frac{1}{\beta(\mathbf{x})} (\nabla + i\mathbf{k}) \cdot \alpha(\mathbf{x}) (\nabla + i\mathbf{k})$ defined on $H_\pi^1(\Omega, \Delta, \alpha)$. The following theorem proved in [10] represents the spectrum of the operator \mathcal{L} using that of $\mathcal{L}_{\mathbf{k}}$.

Theorem 3.1. *For all $\mathbf{k} \in \mathcal{B}$, $\mathcal{L}_{\mathbf{k}}$ has a non-negative discrete spectrum. We can enumerate these eigenvalues in a nondecreasing manner and repeat according to their finite multiplicities as*

$$0 \leq \lambda_1(\mathbf{k}) \leq \lambda_2(\mathbf{k}) \leq \dots \leq \lambda_n(\mathbf{k}) \leq \dots \leq \infty.$$

$\{\lambda_n(\mathbf{k})\}_{n=1}^\infty$ is an infinite sequence with $\lambda_n(\mathbf{k})$ being a continuous function with respect to the wave vector \mathbf{k} and $\lambda_n(\mathbf{k}) \rightarrow \infty$ when $n \rightarrow \infty$. Moreover, the spectrum $\sigma(\mathcal{L})$ of the operator \mathcal{L} is connected to the spectrum $\sigma(\mathcal{L}_{\mathbf{k}})$ of the operators $\mathcal{L}_{\mathbf{k}}$ through

$$\sigma(\mathcal{L}) = \bigcup_{\mathbf{k} \in \mathcal{B}} \sigma(\mathcal{L}_{\mathbf{k}}).$$

In view that $\lambda_n(\mathbf{k}) = \left(\frac{\omega_n(\mathbf{k})}{c}\right)^2$, Theorem 3.1 implies that each band function $\omega_n(\mathbf{k})$ is continuous for all band number $n \in \mathbb{N}^+$.

Next we introduce one of the most important properties of band functions, which lays the main foundation for our proposed interpolation method.

Theorem 3.2 (Piecewise analyticity of the band functions). *2D periodic PhCs band functions are piecewise analytic in the first Brillouin zone \mathcal{B} . In specific, each band function $\omega_n(\mathbf{k})$ is analytic in $\mathcal{B} \setminus X_n$, where X_n is a subset with Lebesgue measure zero composed of branch points and the origin.*

Proof. Our proof is mainly based upon the analyticity of the Bloch variety that was proved in [23, Theorem 4.4.2]. For the sake of completeness, we repeat it in Theorem 3.3. Our proof is inspired by the procedure used in [34], wherein the Bloch wave of Schrödinger equation with periodic potential was considered.

The Bloch variety is defined as

$$B(\mathcal{L}_{\mathbf{k}}) = \{(\mathbf{k}, \lambda) \in \mathbb{R}^3 : \mathcal{L}_{\mathbf{k}} u = \lambda u \text{ admits a nonzero Bloch function } u\}. \quad (3.1)$$

Theorem 3.3 implies that there is an analytic function $D(\mathbf{k}, \lambda)$ on \mathbb{R}^3 such that $B(\mathcal{L}_{\mathbf{k}})$ is its set of zeros, i.e.,

$$B(\mathcal{L}_{\mathbf{k}}) = \{(\mathbf{k}, \lambda) \in \mathbb{R}^3 | D(\mathbf{k}, \lambda) = 0\}. \quad (3.2)$$

We now decompose $B(\mathcal{L}_{\mathbf{k}})$ into two types of sets, where the first type is

$$B^r := \{(\mathbf{k}_0, \lambda_0) \in B(\mathcal{L}_{\mathbf{k}}) : \frac{\partial^{m-1}D}{\partial\lambda^{m-1}} = 0 \text{ in a neighborhood of } (\mathbf{k}_0, \lambda_0) \\ \text{and } \frac{\partial^m D}{\partial\lambda^m}|_{(\mathbf{k}_0, \lambda_0)} \neq 0, \text{ for some } m \in \mathbb{N}^+\}$$

and the second type is $B^s := B(\mathcal{L}_{\mathbf{k}}) \setminus B^r$.

Note that $\lambda_n(\mathbf{k}) \rightarrow \infty$ when $n \rightarrow \infty$ for all $\mathbf{k} \in \mathcal{B}$. To the aim of defining a bounded subset of $B(\mathcal{L}_{\mathbf{k}})$, we introduce

$$B_n := \bigcup_{l=1}^n \{(\mathbf{k}, \lambda_l(\mathbf{k})) | (\mathbf{k}, \lambda_l(\mathbf{k})) \in B(\mathcal{L}_{\mathbf{k}})\}.$$

Analogously, this leads to bounded subsets of B^r and B^s given by

$$B_n^r := B_n \cap B^r \quad \text{and} \quad B_n^s := B_n \cap B^s.$$

Furthermore, let X_n^s be the projection of B_n onto $\lambda = 0$ defined by

$$X_n^s := \{\mathbf{k} \in \mathcal{B} | (\mathbf{k}, \lambda) \in B_n^s \text{ for some } \lambda\}.$$

The definition of B_n^s implies that X_n^s is the set of branch points for the first n bands. Moreover, for any $(\mathbf{k}_0, \lambda_0) \in B_n^s$, there is an integer $m \in \mathbb{N}^+$ such that $(\mathbf{k}_0, \lambda_0) \in \{(\mathbf{k}, \lambda) : D(\mathbf{k}, \lambda) = 0\} \cap \{(\mathbf{k}, \lambda) : \frac{\partial^m D}{\partial\lambda^m} = 0\}$, which is a one-dimensional variety. Hence X_n^s , the projection of B_n^s onto the hyperplane $\lambda = 0$ is a subset of \mathcal{B} with Lebesgue measure zero. Let $\mathbf{k}_0 \in \mathcal{B} \setminus X_n^s$, i.e., $(\mathbf{k}_0, \lambda_l(\mathbf{k}_0)) \in B_n^r$ for $l = 1, \dots, n$. Due to the implicit mapping theorem for analytic functions [21], there is a neighborhood $N(\mathbf{k}_0)$ in which $\lambda_l(\mathbf{k})$ is the unique analytic solution of $\frac{\partial^{m-1}D}{\partial\lambda^{m-1}} = 0$ for some $m \in \mathbb{N}^+$. This implies that each positive band function $\omega_l(\mathbf{k}) = c \cdot \sqrt{\lambda_l(\mathbf{k})}$ is analytic in $\mathcal{B} \setminus X_n^s$. Besides, it is well known that only at the origin the first eigenvalue equals to 0. Thus, we have $X_n = X_n^s \cup \{\mathbf{0}\}$. \square

Theorem 3.3. ([23, Theorem 4.4.2]) *Let L be a general periodic elliptic operator in \mathbb{R}^n , then the complex Bloch variety of L ,*

$$B(L) = \{(\mathbf{k}, \lambda) \in \mathbb{C}^n \times \mathbb{C} \mid \text{the equation } Lu = \lambda u \text{ has a non-zero Bloch function with } \mathbf{k}\},$$

is the set of all zeros of an entire function on \mathbb{C}^{n+1} .

Theorem 3.4 (mentioned in [22] and proved by perturbation theory [20]). *If we only consider one component k_i of the vector $\mathbf{k} = (k_1, k_2)$, then all the positive band functions can be reordered when crossing the branch points such that they are analytic functions with respect to k_i .*

Theorem 3.2 implies that band functions are piecewise analytic with potential singularities occurring at branch points and origin. Theorem 3.4 further shows the analytic continuation of band functions in one variable through branch points. In the following, we will discuss the properties of these singular points and the smoothness of band functions in more details. First we study the limit of eigenfunctions along any band functions.

The variational formulation of (2.13) is: for a given $\mathbf{k} \in \mathcal{B}$, find non-trivial eigenpair $(\lambda, u) \in (\mathbb{R}, H_\pi^1(\Omega))$ satisfying

$$\begin{cases} \int_{\Omega} \alpha(\nabla + i\mathbf{k})u \cdot (\nabla - i\mathbf{k})\bar{v} - \lambda\beta u\bar{v} dx = 0, \text{ for all } v \in H_\pi^1(\Omega) \\ \|u\| = 1. \end{cases} \quad (3.3)$$

Using the sesquilinear forms

$$\begin{aligned} a(u, v) &:= \int_{\Omega} \alpha(\nabla + i\mathbf{k})u \cdot (\nabla - i\mathbf{k})\bar{v} dx, \\ b(u, v) &:= \int_{\Omega} \beta u\bar{v} dx, \end{aligned}$$

(3.3) reads: for a given \mathbf{k} in \mathcal{B} , find non-trivial eigenpair $(\lambda, u) \in (\mathbb{R}, H_\pi^1(\Omega))$ such that

$$\begin{cases} a(u, v) = \lambda b(u, v), \text{ for all } v \in H_\pi^1(\Omega) \\ \|u\| = 1. \end{cases} \quad (3.4)$$

For a given \mathbf{k} , denote the eigenspace of one of the corresponding eigenvalues λ as $E(\lambda)$ and let $\tilde{\mathcal{L}}_{\mathbf{k}}$ be the operator defined on the quotient space $\tilde{H}_\pi^1(\Omega, \Delta, \alpha) := H_\pi^1(\Omega, \Delta, \alpha)/E(\lambda)$ with the same form as $\mathcal{L}_{\mathbf{k}}$. Then the unique different value between the resolvent sets of $\tilde{\mathcal{L}}_{\mathbf{k}}$ and $\mathcal{L}_{\mathbf{k}}$ is λ . More precisely, they have the relation $\rho(\tilde{\mathcal{L}}_{\mathbf{k}}) = \rho(\mathcal{L}_{\mathbf{k}}) \cup \{\lambda\}$, i.e., λ is in the resolvent set of $\tilde{\mathcal{L}}_{\mathbf{k}}$.

In the following, we investigate the regularity of the eigenfunctions.

Theorem 3.5 (Regularity of the eigenfunctions). *For a given band function $\omega_n(\mathbf{k})$, the corresponding normalized eigenfunction $u(x; \mathbf{k})$ can be formulated such that $u(x; \mathbf{k})$ is continuous for all $\mathbf{k} \notin X_n$. In the case that $\mathbf{k} \in X_n$ and multiple-value $\omega_n(\mathbf{k})$ has multiplicity of $2 \leq M \in \mathbb{N}^+$, let $\{u_q(\mathbf{x}; \mathbf{k})\}_{q=1}^M$ be the associated eigenfunctions, then there may exist a jump discontinuity, i.e. there exist $\{c_{i\pm}^q\}_{q=1}^M \subset \mathbb{C}$ such that*

$$\begin{aligned} \lim_{\delta \rightarrow 0} u(\mathbf{x}; \mathbf{k} \pm \delta \mathbf{e}_i) &= \sum_{q=1}^M c_{i\pm}^q u_q(\mathbf{x}; \mathbf{k}), \text{ and } \left\| \sum_{q=1}^M c_{i\pm}^q u_q(\mathbf{x}; \mathbf{k}) \right\| = 1, \\ \text{but } \sum_{q=1}^M c_{i+}^q u_q(\mathbf{x}; \mathbf{k}) &\neq \sum_{q=1}^M c_{i-}^q u_q(\mathbf{x}; \mathbf{k}), \end{aligned}$$

where $\delta > 0$ is a parameter such that $\mathbf{k} \pm \delta \mathbf{e}_i \in \mathcal{B}$, \mathbf{e}_i is the usual unit vector for $i = 1, 2$.

Proof. For the sake of simplicity, we drop the band number for the moment. Let $\omega(\mathbf{k})$ be the band function with $u(\mathbf{x}; \mathbf{k})$ being the associated eigenfunction for any $\mathbf{k} \in \mathcal{B}$. Let the error function be

$$e_i(\delta) := u(\mathbf{x}; \mathbf{k} + \delta \mathbf{e}_i) - u(\mathbf{x}; \mathbf{k}),$$

with $\delta > 0$ being a parameter such that $\mathbf{k} + \delta \mathbf{e}_i \in \mathcal{B}$.

By an application of (2.13) and (3.4), we deduce that the error function $e_i(\delta)$ satisfies the strong formulation

$$(\mathcal{L}_{\mathbf{k}} - \lambda(\mathbf{k})) e_i(\delta) = f(\mathbf{x}; \delta), \quad (3.5)$$

where

$$\begin{aligned} f(\mathbf{x}; \delta) &= (\lambda(\mathbf{k} + \delta \mathbf{e}_i) - \lambda(\mathbf{k})) u(\mathbf{x}; \mathbf{k} + \delta \mathbf{e}_i) - \delta(2k_i + \delta) \frac{1}{\epsilon(\mathbf{x})} u(\mathbf{x}; \mathbf{k} + \delta \mathbf{e}_i) \\ &\quad + \delta i \frac{1}{\beta(\mathbf{x})} \frac{\partial}{\partial x_i} (\alpha(\mathbf{x}) u(\mathbf{x}; \mathbf{k} + \delta \mathbf{e}_i)) + \delta i \frac{1}{\epsilon(\mathbf{x})} \frac{\partial}{\partial x_i} u(\mathbf{x}; \mathbf{k} + \delta \mathbf{e}_i). \end{aligned}$$

The corresponding weak formulation is

$$a(e_i(\delta), v) - \lambda(\mathbf{k}) b(e_i(\delta), v) = g(v; \mathbf{k}, \lambda, u), \quad \text{for all } v \in H_\pi^1(\Omega), \quad (3.6)$$

with $g(v; \mathbf{k}, \lambda, u)$ being

$$\begin{aligned} g(v; \mathbf{k}, \lambda, u) &= (\lambda(\mathbf{k} + \delta \mathbf{e}_i) - \lambda(\mathbf{k})) b(u(\mathbf{x}; \mathbf{k} + \delta \mathbf{e}_i), v) \\ &\quad - \delta(2k_i + \delta) m_\alpha(u(\mathbf{x}; \mathbf{k} + \delta \mathbf{e}_i), v) - \delta m_{\alpha i}(u(\mathbf{x}; \mathbf{k} + \delta \mathbf{e}_i), v), \end{aligned} \quad (3.7)$$

and

$$m_{\alpha i}(u, v) = \int_\Omega i\alpha \left(u \frac{\partial \bar{v}}{\partial x_i} - \bar{v} \frac{\partial u}{\partial x_i} \right) d\mathbf{x}, \quad i = 1, 2, \quad (3.8a)$$

$$m_\alpha(u, v) = \int_\Omega \alpha u \bar{v} d\mathbf{x}. \quad (3.8b)$$

Following the Fredholm–Riesz–Schauder Theory [29], we can derive that for a given \mathbf{k} and a corresponding eigenvalue $\lambda(\mathbf{k})$, Problem (3.5) has a unique solution $e_i(\delta) = (\tilde{\mathcal{L}}_{\mathbf{k}} - \lambda \mathbf{I})^{-1} f(\mathbf{x}; \delta)$ in the quotient space $\tilde{H}_\pi^1(\Omega, \Delta, \alpha)$ which is bounded by

$$\|e_i(\delta)\|_{\tilde{H}_\pi^1(\Omega)} \leq \|(\tilde{\mathcal{L}}_{\mathbf{k}} - \lambda \mathbf{I})^{-1}\| \cdot \|f(\mathbf{x}; \delta)\|. \quad (3.9)$$

Note that $\lambda(\mathbf{k})$ is a continuous function and $u(\mathbf{x}; \mathbf{k}) \in H_\pi^1(\Omega, \Delta, \alpha)$, this leads to $\|f(\mathbf{x}; \delta)\| \rightarrow 0$ as $\delta \rightarrow 0$. Together with (3.9), the error function $e_i(\delta)$ converges to some function in $E(\lambda)$ as $\delta \rightarrow 0$. In a similar manner, we obtain $u(\mathbf{x}; \mathbf{k} - \delta \mathbf{e}_i) - u(\mathbf{x}; \mathbf{k})$ converges to some function in $E(\lambda)$ as $\delta \rightarrow 0$.

Next, we discuss case by case whether a given wave vector \mathbf{k} belongs to the singular sets X_n as defined in Theorem 3.2. Note that the Lebesgue measure of X_n vanishes. If $\mathbf{k} \notin X_n$ and the multiplicity of λ is $1 \leq M \in \mathbb{N}^+$, then the definition of B^r implies the existence of a neighborhood $N(\mathbf{k})$ such that for any $\mathbf{k} \pm \delta \mathbf{e}_i \in N(\mathbf{k})$, the multiplicity of $\lambda(\mathbf{k} \pm \delta \mathbf{e}_i)$ is also M and the corresponding eigenfunctions satisfy for all $1 \leq j \leq M$,

$$\begin{aligned} \lim_{\delta \rightarrow 0} u(\mathbf{x}; \mathbf{k} \pm \delta \mathbf{e}_i) &= \sum_{q=1}^M c_{i\pm}^q u_q(\mathbf{x}; \mathbf{k}), \\ \left\| \sum_{q=1}^M c_{i\pm}^q u_q(\mathbf{x}; \mathbf{k}) \right\| &= 1. \end{aligned}$$

Thus, we can always find a combination of these M normalized eigenfunctions $\{u_j(\mathbf{x}; \mathbf{k})\}_{j=1}^M$ such that there is a normalized eigenfunction $u(\mathbf{x}; \mathbf{k})$, satisfying

$$\lim_{\delta \rightarrow 0} u(\mathbf{x}; \mathbf{k} + \delta \mathbf{e}_i) = \lim_{\delta \rightarrow 0} u(\mathbf{x}; \mathbf{k} - \delta \mathbf{e}_i) = u(\mathbf{x}; \mathbf{k}), \quad i = 1, 2.$$

When $\mathbf{k} \in X_n$ is a singular point and $\lambda(\mathbf{k})$ has multiplicity $M \geq 2$, there is no such kind of neighborhood $N(\mathbf{k})$ such that for any $\mathbf{k} \pm \delta \mathbf{e}_i \in N(\mathbf{k})$, the multiplicity of $\lambda(\mathbf{k} \pm \delta \mathbf{e}_i)$ is also M since the Lebesgue measure of X_n vanishes. Indeed, the multiplicity of $\lambda(\mathbf{k} \pm \delta \mathbf{e}_i)$ is no greater than M . So we cannot always construct such kind of normalized eigenfunctions to ensure the continuity at \mathbf{k} . We only have for any normalized eigenfunction $u(\mathbf{x}; \mathbf{k} \pm \delta \mathbf{e}_i)$ at $\mathbf{k} \pm \delta \mathbf{e}_i$,

$$\lim_{\delta \rightarrow 0} u(\mathbf{x}; \mathbf{k} \pm \delta \mathbf{e}_i) = \sum_{q=1}^M c_{i\pm}^q u_q(\mathbf{x}; \mathbf{k}),$$

with some constant $\{c_{i\pm}^q\}_{q=1}^M \subset \mathbb{C}$ such that $\|\sum_{q=1}^M c_{i\pm}^q u_q(\mathbf{x}; \mathbf{k})\| = 1$ for $i = 1, 2$. This completes the proof. \square

Remark 3.1. When we take the limit of the eigenfunction $u(x; \mathbf{k} + \delta \mathbf{e}_i)$, we need to follow one of the band functions.

We are able now to prove the regularity of band functions.

Theorem 3.6 (Lipchitz continuity of the band functions). *For the case of 2D periodic PhCs, $\omega_n(\mathbf{k}) \in Lip(\mathcal{B}) \cap \mathring{A}(\mathcal{B})$ for all $n \in \mathbb{N}^+$. Here, $Lip(\mathcal{B})$ is the space of Lipchitz continuous functions in the first Brillouin zone \mathcal{B} and $\mathring{A}(\mathcal{B})$ denotes the space of piecewise analytic functions with a zero Lebesgue measure of singular point set.*

Proof. Consider a given regular wave vector \mathbf{k} , and suppose the multiplicity of the eigenvalue $\lambda(\mathbf{k})$ is $M \geq 1$. From Theorem 3.5 we know that there is an eigenfunction $u(\mathbf{x}; \mathbf{k})$ which is continuous in a neighborhood of \mathbf{k} . Taking the partial derivative with respect to k_i for $i = 1, 2$ at \mathbf{k} on both sides of (3.4), this leads to

$$a\left(\frac{\partial u}{\partial k_i}, v\right) - \lambda b\left(\frac{\partial u}{\partial k_i}, v\right) = f^{(1)}\left(v; \mathbf{k}, u, \frac{\partial \lambda}{\partial k_i}\right), \quad (3.10)$$

with

$$f^{(1)}\left(v; \mathbf{k}, u, \frac{\partial \lambda}{\partial k_i}\right) := -m_{\alpha i}(u, v) - 2k_i m_{\alpha}(u, v) + \frac{\partial \lambda}{\partial k_i} b(u, v).$$

Here, the bilinear forms $m_{\alpha i}(\cdot, \cdot)$ and $m_{\alpha}(\cdot, \cdot)$ are defined in (3.8). Note that the kernel of the operator in equation (3.10), i.e., $(\mathcal{L}_k - \lambda \mathbf{I})$, is the eigenspace corresponding to the eigenvalue λ . As a consequence of the Fredholm–Riesz–Schauder theory [29], adding additional orthogonality with this eigenspace implies the existence of a unique solution $\partial_{k_i} u \in H_{\pi}^1(\Omega)$ satisfying

$$\begin{cases} a(\partial_{k_i} u, v) - \lambda b(\partial_{k_i} u, v) = f^{(1)}\left(v; \mathbf{k}, u, \frac{\partial \lambda}{\partial k_i}\right) \text{ for all } v \in H_{\pi}^1(\Omega), \\ \langle \partial_{k_i} u, u_p \rangle = 0 \text{ for } p = 1, \dots, M. \end{cases} \quad (3.11)$$

where $\{u_p\}_{p=1}^M$ is a set of basis of the eigenspace. Let the test function $v := u$, we obtain

$$a(\partial_{k_i} u, u) - \lambda b(\partial_{k_i} u, u) = \overline{a(u, \partial_{k_i} u) - \lambda b(u, \partial_{k_i} u)} = f^{(1)}\left(u; \mathbf{k}, u, \frac{\partial \lambda}{\partial k_i}\right) = 0. \quad (3.12)$$

Then we can solve for $\frac{\partial \lambda}{\partial k_i}$ using

$$f^{(1)}\left(u; \mathbf{k}, u, \frac{\partial \lambda}{\partial k_i}\right) = 0,$$

which results in

$$\frac{\partial \lambda}{\partial k_i} = \frac{2k_i m(u, u) + m_{\alpha i}(u, u)}{b(u, u)}. \quad (3.13)$$

Consequently, $\frac{\partial \lambda}{\partial k_i}$ is uniformly bounded. Moreover, from the above formulation of $\frac{\partial \lambda}{\partial k_i}$ as well as Theorem 3.5, we can derive the left and right partial derivative on a given singular wave vector \mathbf{k}_0 with the multiplicity of the corresponding eigenvalue larger than one:

$$\begin{aligned} \left. \frac{\partial_{\pm} \lambda}{\partial k_i} \right|_{\mathbf{k}=\mathbf{k}_0} &= \lim_{\delta \rightarrow \pm 0} \left. \frac{2k_i m(u, u) + m_{\alpha i}(u, u)}{b(u, u)} \right|_{\mathbf{k}=\mathbf{k}_0+\delta \mathbf{e}_i} \\ &= \frac{2k_i \sum_{q=1}^M \sum_{p=1}^M c_{i\pm}^q c_{i\pm}^p (m(u_q(\mathbf{x}; \mathbf{k}), u_p(\mathbf{x}; \mathbf{k})) + m_{\alpha i}(u_q(\mathbf{x}; \mathbf{k}), u_p(\mathbf{x}; \mathbf{k})))}{\sum_{q=1}^M \sum_{p=1}^M c_{i\pm}^q c_{i\pm}^p b(u_q(\mathbf{x}; \mathbf{k}), u_p(\mathbf{x}; \mathbf{k}))}, \end{aligned} \quad (3.14)$$

where M is the multiplicity of $\lambda(\mathbf{k}_0)$, the associated eigenfunctions $\{u_q(\mathbf{x}; \mathbf{k}_0)\}_{q=1}^M$ and complex values $\{c_{i\pm}^q\}_{q=1}^M \subset \mathbb{C}$ satisfy Theorem 3.5 for $i = 1, 2$.

The first derivative of each positive band function at regular points can be easily derived from the relation $\lambda(\mathbf{k}) = \left(\frac{\omega(\mathbf{k})}{c}\right)^2$. Now we can get that band functions are continuous but not continuously differentiable. More precisely, each band function is differentiable almost everywhere, and the partial derivative is bounded. Thus, we prove this theorem. \square

Remark 3.2. *As is shown in [22], we can further prove that the eigenfunctions can indeed be organized to be continuously differentiable of any degree at all non-singular points. However, the properties of eigenfunctions at singular points are not discussed in the aforementioned paper. The authors conjectured that there may exist an ordering of band functions such that the corresponding eigenfunctions are also continuously differentiable at singular points.*

4 Numerical schemes

As shown in the previous section, band functions of 2D periodic PhCs are real-valued, non-negative, continuous, and piecewise analytic within the first Brillouin zone. Besides, in 2D PhCs with symmetrical structures, there exists a triangular area within the first Brillouin zone, which is the so-called irreducible Brillouin zone (IBZ). All other points in the first Brillouin zone can be transferred into the irreducible Brillouin zone by mirror symmetry or rotational symmetry, so the eigenvalues at these points are also the same as the eigenvalues of the corresponding points in the IBZ, which will be proved in details in Section A. Hence, what we focus on is the band function approximation in the triangular domain, i.e., the irreducible Brillouin zone or within the quadrilateral domain, which includes the irreducible Brillouin zone and its mirror symmetric area along one of its edges.

Based on the properties of band functions we derive, we exploit in this work the band functions reconstruction based upon Lagrange interpolation on a certain domain \mathcal{B} . In specific, given a set of N distinct sampling points $\{\mathbf{x}_i\}_{i=1}^N$ and approximate band function values $\{f_i\}_{i=1}^N$ for a given band number, the corresponding Lagrange interpolation $\mathbf{L}f$ is a linear combination of the Lagrange polynomials $\{l_i(\mathbf{x})\}_{i=1}^N$ for those sampling points satisfying $l_i(\mathbf{x}_j) = \delta_{ij}$ such that it interpolates the data, i.e.,

$$\mathbf{L}f = \sum_{i=1}^N f_i l_i(\mathbf{x}). \quad (4.1)$$

We refer to [5, Section 2] for more details on Lagrange interpolation. The approximate band function values are obtained by solving the eigenvalue problem (2.13) numerically.

As is known that the optimal nodal set within a triangle in uniform norm is characterized by minimizing the so-called Lebesgue constant $\Gamma_{N-1}(\{\mathbf{x}_i\}_{i=1}^N)$, defined by

$$\Gamma_{N-1}(\{\mathbf{x}_i\}_{i=1}^N) := \max_{x \in T} \sum_{i=1}^N |l_i(\mathbf{x})|. \quad (4.2)$$

Let $P_n(\mathcal{B})$ be the polynomial space with degree at most n such that $N := \dim(P_n(T)) = \frac{1}{2}(n+1)(n+2)$. Then we have the following near-best approximation which bounds our interpolation error through the Lebesgue constant [33, Theorem 15.1],

$$\sup_{\mathbf{x} \in \mathcal{B}} |f(\mathbf{x}) - \mathbf{L}f(\mathbf{x})| \leq (1 + \Gamma_{N-1}(\{\mathbf{x}_i\}_{i=1}^N)) \inf_{p_n \in P_n(\mathcal{B})} \sup_{\mathbf{x} \in \mathcal{B}} |f(\mathbf{x}) - p_n(\mathbf{x})|.$$

The minimization of (4.2) is not trivial to solve for any type of the domains in more than one dimension. Since the denominator of the Lagrange polynomials vanishes on a subset of T , the Lebesgue constant is not continuous with respect to the point set $\{\mathbf{x}_i\}_{i=1}^N$ in T^N . Besides, $\Gamma_{N-1}(\{\mathbf{x}_i\}_{i=1}^N)$ is very sensitive to the location of the interpolation points, which makes the minimization procedure subtle. Although there have been several attempts to produce nodal sets using direct and indirect methods to minimize the Lebesgue constant, for example, [13] directly minimizes the Lebesgue constant with Fekete points as their initial guess and [6] minimizes norms of the Lagrange interpolation operator, which also yields small Lebesgue constant, nor are we able to find the exact optimal points. Thus, the question of how to sample points in a triangle which are suitable for polynomial interpolation is still an open question.

Since in the multivariate case, the optimal Lagrange interpolant is hard to determine, our aim is to find a suitable sampling point set, on which our Lagrange interpolation performs well when dealing with the band function reconstruction.

4.1 Sampling points in triangle

To standardize the problem, let the right isosceles triangle T be the reference triangle,

$$T := \{\mathbf{x} = (x, y) : 0 \leq x \leq 1, 0 \leq y \leq 1 - x\},$$

and let $P_n(T)$ be the space of polynomials on T with degree at most n ,

$$P_n(T) = \text{span}\{x^i y^j, \quad i + j \leq n\}.$$

In the following, we introduce several sampling methods on this reference triangle T .

Mean optimal points

The mean optimal nodal set is defined by minimizing a norm related to the Lagrange interpolation operator \mathbf{L} , which takes the form [6]

$$\|\mathbf{L}\|_2 := \int_T \sum_{i=1}^N |l_i(\mathbf{x})|^2 d\mathbf{x}. \quad (4.3)$$

Here, $\{l_i(\mathbf{x})\}_{i=1}^N$ is defined as in (4.2). Compared with (4.2), the minimization of (4.3) involves less computational complexity and thus more favorable. Indeed, suppose $\{p_i(\mathbf{x})\}_{i=1}^N$ is a set of standard orthogonal polynomials on the triangle T with degree at most n , i.e., $\int_T p_i(\mathbf{x})p_j(\mathbf{x})d\mathbf{x} = \delta_{ij}$ for all $i, j = 1, \dots, N$. Then for any given point set $\{\mathbf{x}_j\}_{j=1}^N$, the Lagrange polynomials can be expressed as $l_k(\mathbf{x}) = \sum_{i=1}^N a_{ki}p_i(\mathbf{x})$ with some constant $\{a_{ki}\}_{k,i=1}^N$, which allows (4.3) to be expressed as $\|\mathbf{L}\|_2 = \sum_{k=1}^N \sum_{i=1}^N |a_{ki}|^2$. In comparison, the calculation of $\Gamma_{N-1}(\{\mathbf{x}_i\}_{i=1}^N)$ is equivalent to the calculation of $\max_{x \in T} \sum_{k=1}^N |\sum_{i=1}^N |a_{ki}p_i(\mathbf{x})|$, which has more computational complexity. Numerical results show that $\|\mathbf{L}\|_2 \setminus \Gamma_{N-1}(\{\mathbf{x}_i\}_{i=1}^N)$ is not large and the performance of this kind of point set is nearly optimal.

Fekete points

Fekete point set [3] is another kind of nearly optimal nodal point set which maximizes the absolute value of the determinant of Vandermonde matrix $V(\mathbf{x}_1, \mathbf{x}_2, \dots, \mathbf{x}_N)$,

$$\max_{\{\mathbf{x}_1, \mathbf{x}_2, \dots, \mathbf{x}_N\} \subset T} |\det(V(\mathbf{x}_1, \mathbf{x}_2, \dots, \mathbf{x}_N))|. \quad (4.4)$$

Here, $V(\mathbf{x}_1, \mathbf{x}_2, \dots, \mathbf{x}_N)$ is of size $N \times N$ with entries

$$V_{ij} = g_j(\mathbf{x}_i) \text{ for } i, j = 1, \dots, N.$$

$\{g_i\}_{i=1}^N$ denotes a set of basis functions in $P_n(T)$. Note that $\det(V)$ can be regarded as a polynomial function of $(\mathbf{x}_1, \dots, \mathbf{x}_n)$, which implies the existence of Fekete points for a given compact set T . Note also that Problem (4.4) involves less computational complexity than Problem (4.2). As the first attempt, Bos [3] constructed the Fekete point set up to the 7th order, which was further extended up to degree 13 [6] and 18 in a triangle, respectively.

Improved Lobatto grid

The improved Lobatto grid is proposed in [2] as an improvement of the original Lobatto grid, which composes of (ξ_i, η_j) defined by

$$\xi_i = \frac{1}{3}(1 + 2v_j - v_i - v_k), \eta_j = \frac{1}{3}(1 + 2v_i - v_j - v_k) \text{ for } i = 1, \dots, n+1 \text{ and } j = 1, \dots, n+2-i.$$

Here, $v_i = \frac{1}{2}(1+t_i)$, t_i denotes the zeros of the n th degree Lobatto polynomials and $k = n+3-i-j$.

This proposed point set utilizes the zeros of Lobatto polynomials which are optimal for 1D interpolation [8]. It is generated by deploying Lobatto interpolation nodes along the three edges of the triangle, and then computing interior nodes by averaged intersections to achieve three-fold rotational symmetry. The symmetry of the distribution with respect to the three vertices is a significant improvement of the original Lobatto grid. Its straightforward implementation makes it an attractive choice, and numerical results show that the Lebesgue constant for this point set is competitive with the above mentioned two point sets.

The following figures show the comparison of mean optimal points, Fekete points, and the improved Lobatto grid for $n = 4, 8$.

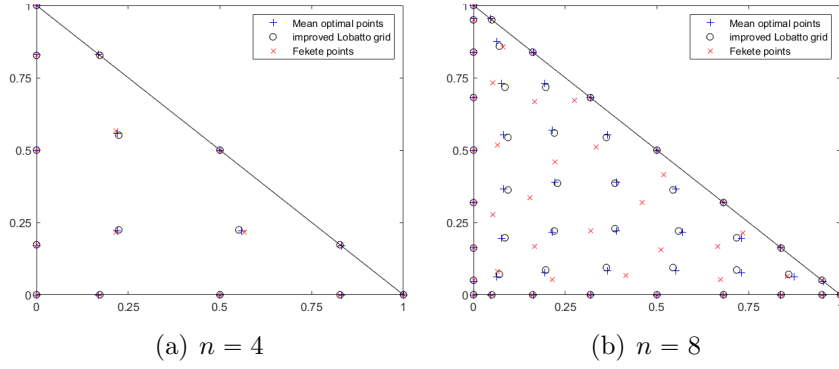


Figure 2: Mean optimal points, Fekete points, and improved Lobatto grid for $n = 4, 8$.

Remark 4.1 (Lebesgue constants for mean optimal points, Fekete points and improved Lobatto grid). *Although there is no rigorous proof on the boundedness of the Lebesgue constants for mean optimal points, Fekete points and improved Lobatto grid, numerical evidence [6, 32, 2] suggests that their Lebesgue constants are proportional to \sqrt{N} .*

4.2 Sampling points in quadrilateral

For a quadrilateral, we will first project it into the unit square $S := [-1, 1]^2$ by projective mapping [12] and then consider the polynomial space with two variables and degree at most n in each variable, i.e.

$$P_n(S) = \text{span}\{x^i y^j, \quad i, j \leq n\}.$$

It is well known that in 1D case, interpolation using the zeros of Chebyshev polynomials is close to optimal. So in the case of unit square, we mainly consider the following two sampling point sets with tensor product:

The Chebyshev points of the first kind (Cheb1) in the interval $[-1, 1]$ are the zeros of the Chebyshev polynomial of the first kind $T_{n+1}(x)$,

$$x_k = \cos \frac{2k+1}{2n} \pi, \quad k = 0, \dots, n.$$

The Chebyshev points of the second kind (Cheb2) in the interval $[-1, 1]$ are the zeros of the Chebyshev polynomial of the second kind $U_{n-1}(x)$ times $(x^2 - 1)$, i.e.,

$$x_i = \cos \left(\frac{i}{n} \pi \right), \quad i = 0, \dots, n.$$

Figure 3 demonstrates the comparison of Cheb1 and Cheb2 for $n = 4$ and $n = 8$ after using tensor product to expand them to the unit square.

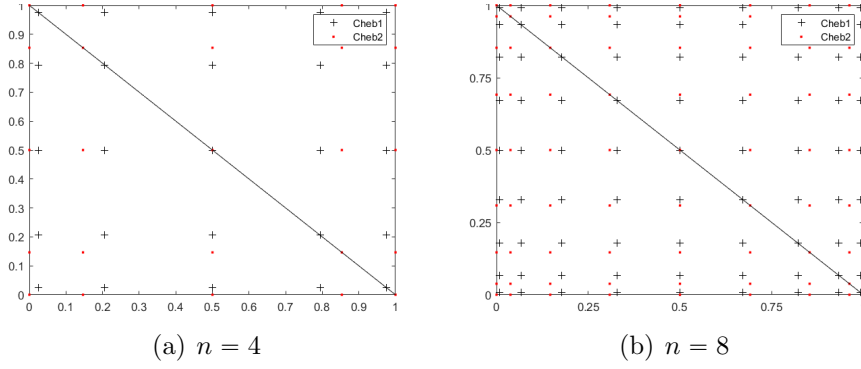


Figure 3: Cheb1 and Cheb2 with tensor product for $n = 4, 8$.

Remark 4.2 (Lebesgue constants for Cheb1 and Cheb2). *Since the Lebesgue constants of Cheb1 and Cheb2 are both proportional to $\log(N)$ [15], where $N = n + 1$ is the dimension of the polynomial space in $[-1, 1]$, the Lebesgue constants of our nodal point sets are proportional to $(\log(N))^2$, where $N = (n + 1)^2$ is the dimension of the polynomial space with two variables and degree at most n in each variable.*

Remark 4.3 (Comparison of computational complexity). *It is worth noticing that the computation cost involved in the eigenvalue problem is consistent by using all these five kinds of sampling points, even though the number of Chebyshev points is almost twice as the number of those three kinds of sampling points within the triangular area. That is because of the mirror and rotational symmetry mentioned earlier. For example, in Figure 3(a), we have 25 Chebyshev points, but we only need to compute eigenvalues at 15 of them within the right isosceles triangle.*

Remark 4.4. *Considering the importance of the edges of the irreducible Brillouin zone, we can further speculate that the performance of Cheb2 is better than that of Cheb1. The numerical results presented in the next section can further confirm this speculation.*

5 Numerical experiments

To demonstrate the performance of our proposed methods (4.1) together with the sampling methods presented above, we mainly consider PhCs with a square unit cell as in Figure 4 and a hexagonal unit cell as in Figure 5. We calculate the eigenvalue problem for a given sampling point using the conforming Galerkin Finite Element method.



Figure 4: 2D PhCs of square lattice with unit cell Ω and its corresponding first Brillouin zone. The irreducible Brillouin zone is the blue area with vertices $\Gamma = (0, 0)$, $X = \frac{1}{a}(\pi, 0)$, $M = \frac{1}{a}(\pi, \pi)$.

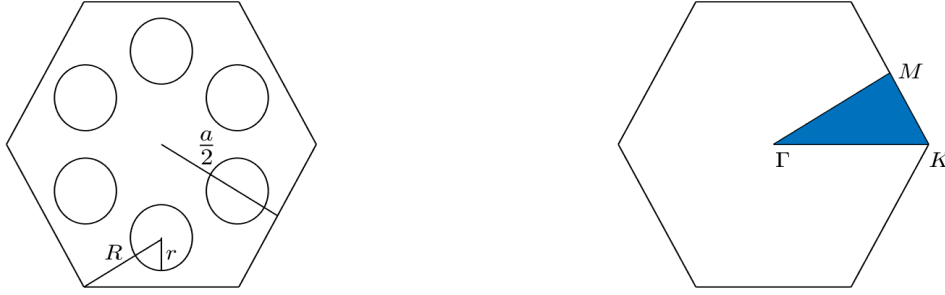


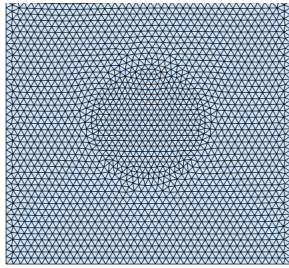
Figure 5: 2D PhCs of hexagonal lattice with unit cell Ω and its corresponding first Brillouin zone. The irreducible Brillouin zone is the blue area with vertices $\Gamma = (0, 0)$, $K = \frac{1}{a}(\frac{4}{3}\pi, 0)$, $M = \frac{1}{a}(\pi, \frac{\sqrt{3}}{3}\pi)$.

Due to the high contrast between the relative permittivity of the circular medium and its external medium, we utilize a fitted mesh generated by *distmesh2d* provided by Persson and Strang to avoid the stabilization issue occurred when an unfitted mesh is used. The mesh generated by this kind of method is shown in Figures 6(a) and 6(b), which is denoted as \mathcal{T}_h with mesh size $h = 0.025a$ for square lattice and $h = 0.05a$ for hexagonal lattice. The associated conforming piecewise affine space is

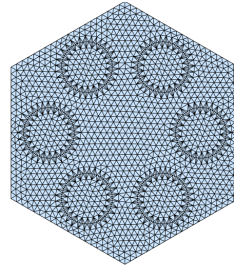
$$V_h = \{v_h \in C(\bar{\Omega}) : v_h|_K \in P_1(K) \forall K \in \mathcal{T}_h\}.$$

Given $\mathbf{k} \in \mathcal{B}$, the conforming Galerkin Finite Element approximation to Problem (3.4) reads as finding non-trivial eigenpair $(\lambda_h, u_h) \in (\mathbb{R}, V_h)$, satisfying

$$\begin{cases} a(u_h, v_h) = \lambda b(u_h, v_h) \text{ for all } v \in V_n \\ \|u_h\| = 1. \end{cases} \quad (5.1)$$



(a) Square lattice #DOFs=2107



(b) Hexagonal lattice #DOFs=1781

Figure 6: Discretization of the unit cell Ω by *distmesh2d*.

In both cases, the irreducible Brillouin zone is a triangle. We map it into the right isosceles triangle and use 253 evenly distributed points shown in Figure 7(a) and Figure 7(b) to measure the interpolation error as well as the quality of our sampling points. The error rate (relative error) in eigenfrequency is defined as

$$e_i^k = \frac{|\omega_i(\mathbf{k}) - \hat{\omega}_i(\mathbf{k})|}{\hat{\omega}_i(\mathbf{k})}, \quad i = 1, \dots, 6.$$

Here $\hat{\omega}_i(\mathbf{k})$ is the eigenfrequency obtained directly by the conforming Galerkin Finite Element method over these 253 points using the same mesh on the unit cell Ω , and $\omega_i(\mathbf{k})$ is the polynomial interpolation result.

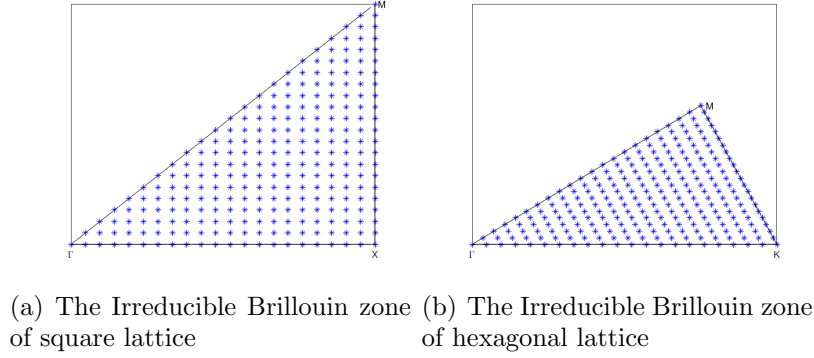


Figure 7: Points used to measure error

5.1 Numerical tests with square lattice in Figure 4

In this section, we are concerned with square lattice as in Figure 4, wherein the lattice vectors are $\mathbf{a}_1 = a(0, 1)^T$, and $\mathbf{a}_2 = a(1, 0)^T$ with a positive parameter a . The circle area has radius $r = 0.2a$ and $\epsilon = 8.9$ (as for alumina) which is embedded in air ($\epsilon = 1$). In this case, due to the symmetry of the first Brillouin zone, we can restrict k in the irreducible Brillouin zone.

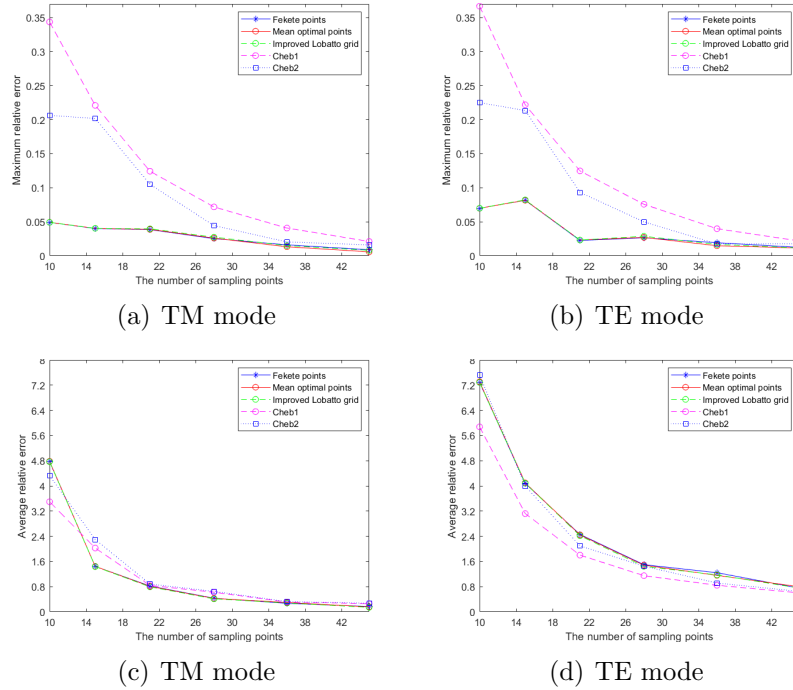


Figure 8: Maximum and average relative error of the first six eigenfrequencies generated by Lagrange interpolation.

The performance of Lagrange interpolation on those five kinds of sampling points is shown in Figure 8. Figure 9 depicts the band structure along the edges of the irreducible Brillouin zone.

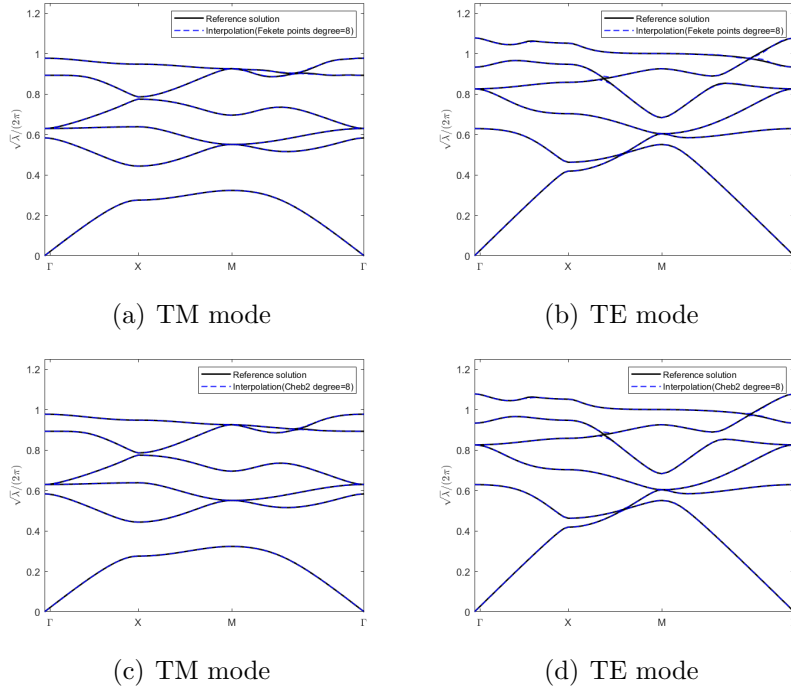


Figure 9: Band functions along the edges of the irreducible Brillouin zone.

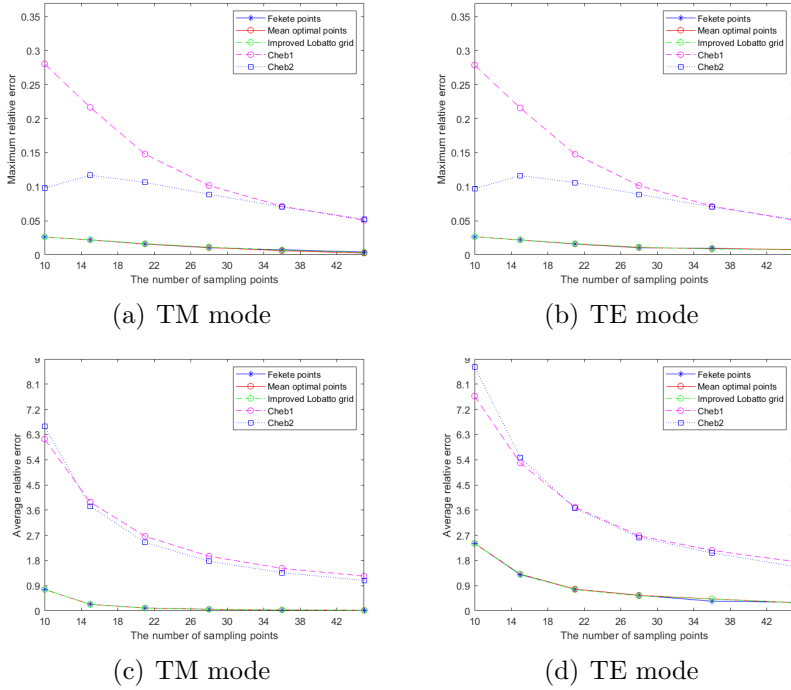


Figure 10: Maximum and average relative error of the first six eigenfrequencies generated by Lagrange interpolation.

5.2 Numerical tests with hexagonal lattice in Figure 5

In this section, we focus on another kind of 2D PhCs which has infinite periodic hexagonal lattice. As shown in Figure 5, the unit cell of our photonic crystal is composed of six cylinders of dielectric material with dielectric constant $\epsilon = 8.9$ embedded in the air, and the lattice vectors $\mathbf{a}_1, \mathbf{a}_2$ are chosen to be $\mathbf{a}_1 = a(1, 0)^T$, $\mathbf{a}_2 = a(\frac{1}{2}, \frac{\sqrt{3}}{2})^T$, with lattice constant $a = 3R$, R is the length of hexagon edges and $r = \frac{1}{3}R$ is the radius of cylinders. In this case, due to the symmetry of the first Brillouin zone, we can also restrict \mathbf{k} in the irreducible Brillouin zone.

Figure 10 displays the Lagrange interpolation error on those five kinds of sampling points in terms of the number of sampling points inside the irreducible Brillouin zone. We observe from Figure 8 and Figure 10 that the error decays fast with the number of sampling points. When we take 45 sampling points inside the irreducible Brillouin zone to reconstruct band functions, the maximum relative error can be within 1% depending on the choice of sampling methods as well as the smoothness of the band functions. For example, the interpolation error of the band functions in the case of hexagonal unit cell is generally smaller than that of the square unit cell since the first six band functions are smoother in the former case. In comparison, there are more singularities in the latter case, which result in larger interpolation errors and thus slow down the convergence rate. We also observe that the error of the first three sampling methods (Fekete points, mean optimal points, improved Lobatto grid) in both cases, are similar or smaller than Cheb1 and Cheb2.

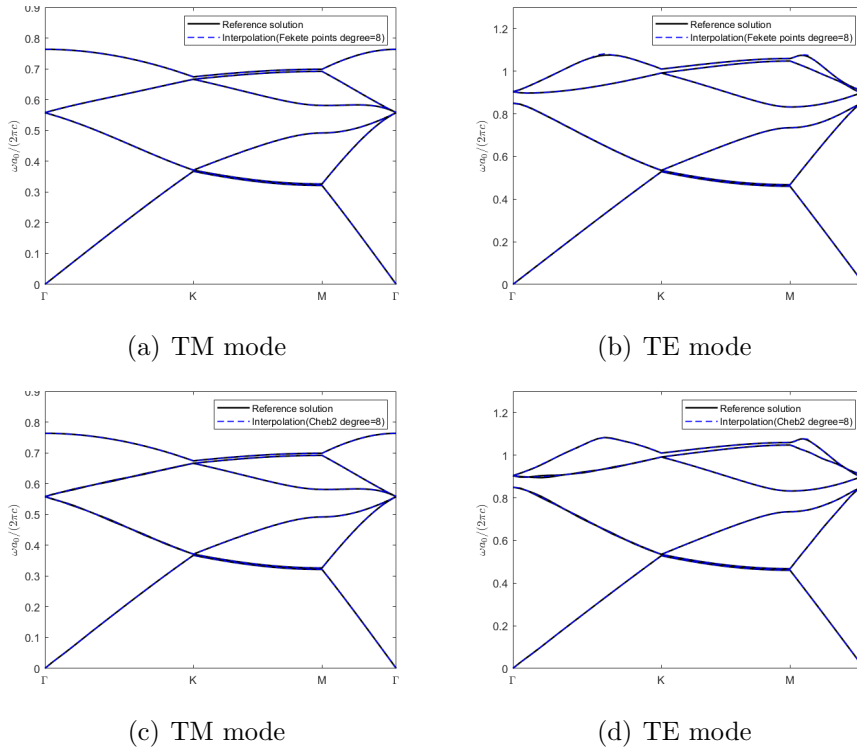


Figure 11: Band functions along the edges of the irreducible Brillouin zone.

Figure 11 illustrates the band structure along the edges of the irreducible Brillouin zone. Together with Figure 9, we conclude that all those five methods can provide reasonably good reconstruction. Figure 12 shows a zoomed-in view of some special points of Figure 9 and Figure 11. We can observe that the area with large interpolation error is clearly the area where the

adjacent band functions are very close, which is consistent with the conclusion we have drawn before that the branch points are singular points.

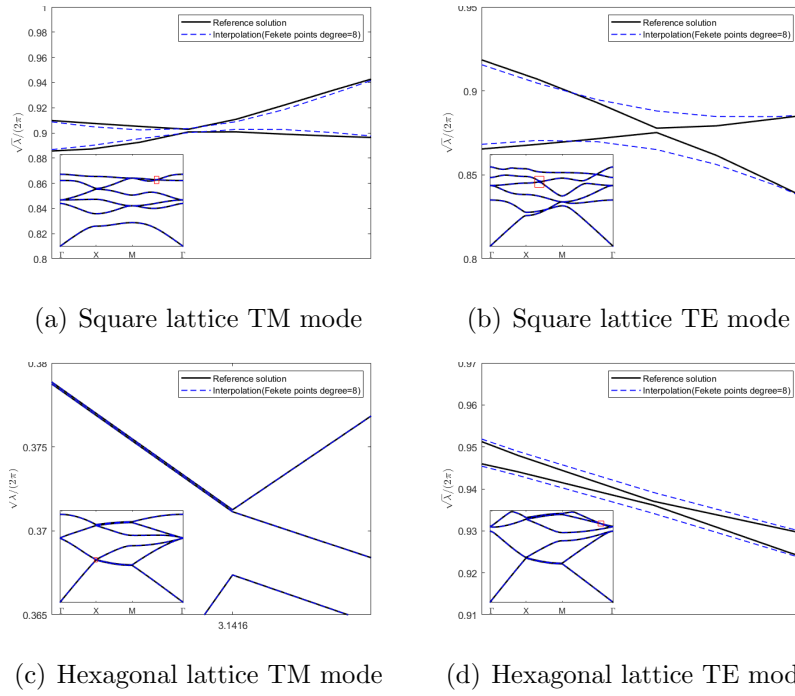


Figure 12: Zoom in on the interpolation results within the red box area.

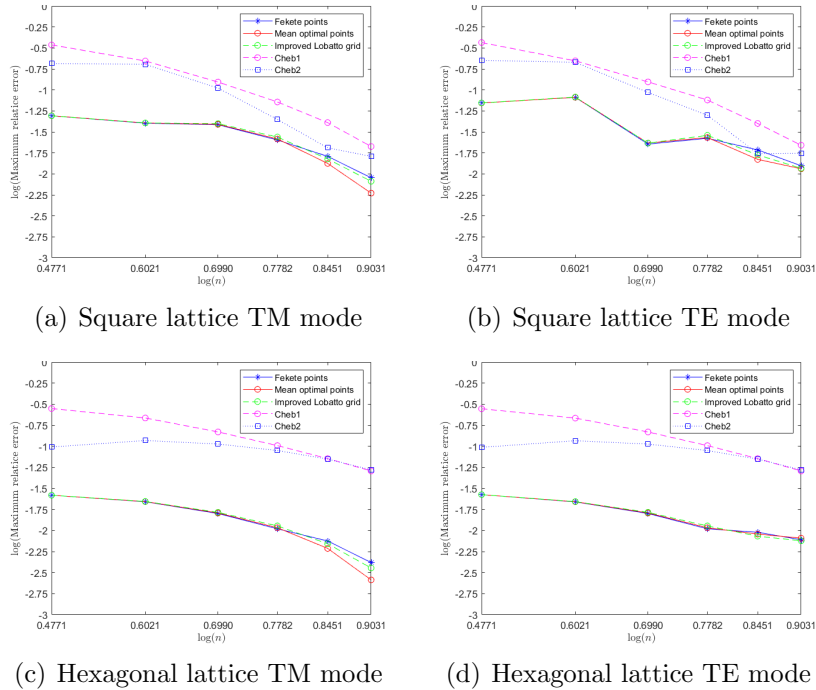


Figure 13: Maximum and average relative error of the first six eigenfrequencies generated by Lagrange interpolation.

In Figure 13, we depict the Log-log graph for the order of convergence. From these results,

we can see that the convergence rate of the first three sampling methods (Fekete points, mean optimal points, improved Lobatto grid), are similar and a bit slower than that of Cheb1 and Cheb2.

6 Conclusion

In this paper, we analyze the properties of two-dimensional photonic band functions. In contrast to the traditional sampling algorithms based upon global polynomial interpolation, which are limited to the edges of the irreducible Brillouin zone, we propose an efficient and accurate global approximation algorithm for computing band functions over the whole first Brillouin zone. We choose Lagrange interpolation since it is easier to work with and can provide an excellent approximation. Regarding the selection of sampling points, we consider five different sampling algorithms to select suitable interpolation points in the first Brillouin zone or the irreducible Brillouin zone. Numerical tests demonstrate all those five kinds of sampling methods can provide us with accurate and competitive sampling strategy for interpolation over the first Brillouin zone or irreducible Brillouin zone to reconstruct PhCs band functions. We focus on sampling algorithms based upon global polynomial interpolation in this paper since this is the current start-of-the-art. Since the band functions are piecewise analytic, we will investigate adaptive sampling algorithm based upon piecewise polynomial interpolation in the future.

Acknowledgments

G.L. acknowledges support from Newton International Fellowships Alumni following-on funding awarded by The Royal Society and Early Career Scheme (Project number: 27301921), RGC, Hong Kong.

A Proof of the symmetry

Consider the 2D PhCs shown in Figure 4, which has a symmetric structure about $y = x$. Suppose the lattice vectors are $\mathbf{a}_1 = a(0, 1)^T$, and $\mathbf{a}_2 = a(1, 0)^T$ with a positive parameter a , then we define $\mathbf{a} := (\mathbf{a}_1, \mathbf{a}_2)$. Let \mathbf{T}_n denote a translation operator which takes the form

$$\mathbf{T}_n f(\mathbf{x}) = f(\mathbf{x} + \mathbf{n} \cdot \mathbf{a}),$$

where $\mathbf{n} = (n_1, n_2) \in \mathbb{Z}^2$, and $\mathbf{n} \cdot \mathbf{a} := n_1 \mathbf{a}_1 + n_2 \mathbf{a}_2$.

Lemma A.1. (proved in [26]) *If two operators \hat{A}, \hat{B} commute with each other,*

$$\hat{A}\hat{B} - \hat{B}\hat{A} = 0,$$

then we can come up with a set of basis states that are eigenfunctions of both \hat{A} and \hat{B} .

Given that the operator \mathcal{L} is invariant for these kinds of translations, it commutes with \mathbf{T}_n , i.e.

$$\mathbf{T}_n \mathcal{L} - \mathcal{L} \mathbf{T}_n = 0.$$

Hence, \mathcal{L} has the same eigenfunctions with $\mathbf{T}_{\mathbf{n}}$. Besides, it is easy to find that all of the translation operators commute with each other. So let's start with the eigenvalues of $\mathbf{T}_{\mathbf{n}}$:

$$\mathbf{T}_{\mathbf{n}}\Psi(\mathbf{x}) = \Psi(\mathbf{x} + \mathbf{n} \cdot \mathbf{a}) = \lambda_{\mathbf{n}}\Psi(\mathbf{x}). \quad (\text{A.1})$$

Since the translation operators are additive operators, we obtain

$$\lambda_{\mathbf{n}_1}\lambda_{\mathbf{n}_2} = \lambda_{\mathbf{n}_1+\mathbf{n}_2}. \quad (\text{A.2})$$

From the above equation (A.2), we can get that the eigenvalues of the translation operators have the form $\lambda_{\mathbf{n}} = e^{\mathbf{s} \cdot (\mathbf{n} \cdot \mathbf{a})}$, where $\mathbf{s} \in \mathbb{C}^2$. If we use the normalization condition over the primitive cell Ω , i.e.

$$1 = \int_{\Omega} |\Psi(\mathbf{x})|^2 d\mathbf{x} = \int_{\Omega} |\mathbf{T}_{\mathbf{n}}\Psi(\mathbf{x})|^2 d\mathbf{x} = |\lambda_{\mathbf{n}}|^2 \int_{\Omega} |\Psi(\mathbf{x})|^2 d\mathbf{x},$$

we derive

$$1 = |\lambda_{\mathbf{n}}|^2.$$

Hence, $\mathbf{s} = i\mathbf{k}$ with $\mathbf{k} \in \mathbb{R}^2$, and the eigenvalues of the translation operator $\mathbf{T}_{\mathbf{n}}$ take the form $e^{i\mathbf{k} \cdot (\mathbf{n} \cdot \mathbf{a})}$.

Now suppose \mathbf{M} is an operator that makes coordinate vectors symmetric about $y = x$, then we operate this operator on any mode of the system, $U(\mathbf{x})$, we obtain

$$\begin{aligned} \mathbf{M}(\mathcal{L}U(\mathbf{x})) &= \mathbf{M}\left(-\frac{1}{\beta(\mathbf{x})}\nabla \cdot \alpha(\mathbf{x})\nabla U(\mathbf{x})\right) \\ &= \left(-\frac{1}{\beta(\mathbf{x})}\nabla \cdot \alpha(\mathbf{x})\nabla\right)\mathbf{M}U(\mathbf{x}) \\ &= \mathcal{L}(\mathbf{M}U(\mathbf{x})) \\ &= \left(\frac{\omega}{c}\right)^2(\mathbf{M}U). \end{aligned}$$

So if U is a mode with frequency ω , then $\mathbf{M}U$ is also a mode with frequency ω . Moreover, since the translation operators $\mathbf{T}_{\mathbf{n}}$ commute with \mathcal{L} and share a set of eigenfunctions with \mathcal{L} , we get that $\mathbf{M}U$ is also an eigenfunction of $\mathbf{T}_{\mathbf{n}}$. Because the eigenvalues of the translation operators take the form $e^{i\mathbf{k} \cdot (\mathbf{n} \cdot \mathbf{a})}$, we obtain

$$\begin{aligned} \mathbf{T}_{\mathbf{n}}(\mathbf{M}U) &= \mathbf{M}(\mathbf{T}_{\mathbf{M}^{-1}\mathbf{n}}U) = \mathbf{M}(e^{i\mathbf{k} \cdot \mathbf{M}^{-1}(\mathbf{n} \cdot \mathbf{a})}U) \\ &= e^{i\mathbf{M}\mathbf{k} \cdot (\mathbf{n} \cdot \mathbf{a})}\mathbf{M}U. \end{aligned} \quad (\text{A.3})$$

So following Bloch's theorem, $\mathbf{M}U$ is the Bloch state with wave vector $\mathbf{M}\mathbf{k}$, having the same frequency ω with U .

Now we conclude that if we consider the photonic crystal with lattice shown in Figure 4, which has a symmetric structure about $y = x$, then $\mathbf{k} = (k_1, k_2)$ shares the same eigenvalue with $\hat{\mathbf{k}} = (k_2, k_1)$. This conclusion can be easily generalized to other symmetries.

References

- [1] Gang Bao, Lawrence Cowsar, and Wen Masters. *Mathematical modeling in optical science*. SIAM, 2001.
- [2] MG Blyth and C Pozrikidis. “A Lobatto interpolation grid over the triangle”. In: *IMA journal of applied mathematics* 71.1 (2006), pp. 153–169.
- [3] L Bos. “On certain configurations of points in R^n which are unisolvent for polynomial interpolation”. In: *Journal of approximation theory* 64.3 (1991), pp. 271–280.
- [4] Len Bos et al. “Computing multivariate Fekete and Leja points by numerical linear algebra”. In: *SIAM Journal on Numerical Analysis* 48.5 (2010), pp. 1984–1999.
- [5] Claudio Canuto et al. *Spectral methods: fundamentals in single domains*. Springer Science & Business Media, 2007.
- [6] Qi Chen and Ivo Babuška. “Approximate optimal points for polynomial interpolation of real functions in an interval and in a triangle”. In: *Computer Methods in Applied Mechanics and Engineering* 128.3-4 (1995), pp. 405–417.
- [7] RV Craster et al. “Dangers of using the edges of the Brillouin zone”. In: *Physical Review B* 86.11 (2012), p. 115130.
- [8] Leopold Fejér. “Lagrangesche Interpolation und die zugehörigen konjugierten Punkte”. In: *Mathematische Annalen* 106.1 (1932), pp. 1–55.
- [9] Stefano Giani and Ivan G Graham. “Adaptive finite element methods for computing band gaps in photonic crystals”. In: *Numerische Mathematik* 121.1 (2012), pp. 31–64.
- [10] Izrail’ Markovich Glazman. *Direct methods of qualitative spectral analysis of singular differential operators*. Vol. 2146. Israel Program for Scientific Translations, 1965.
- [11] JM Harrison et al. “On occurrence of spectral edges for periodic operators inside the Brillouin zone”. In: *Journal of Physics A: Mathematical and Theoretical* 40.27 (2007), p. 7597.
- [12] Paul Heckbert. “Projective mappings for image warping”. In: *Image-Based Modeling and Rendering* 869 (1999).
- [13] Wilhelm Heinrichs. “Improved Lebesgue constants on the triangle”. In: *Journal of Computational Physics* 207.2 (2005), pp. 625–638.
- [14] Mahmoud I Hussein. “Reduced Bloch mode expansion for periodic media band structure calculations”. In: *Proceedings of the Royal Society A: Mathematical, Physical and Engineering Sciences* 465.2109 (2009), pp. 2825–2848.
- [15] Bayram Ali Ibrahimoglu. “Lebesgue functions and Lebesgue constants in polynomial interpolation”. In: *Journal of Inequalities and Applications* 2016.1 (2016), pp. 1–15.
- [16] John David Jackson. *Classical electrodynamics*. 1999.
- [17] John D Joannopoulos et al. “Molding the flow of light”. In: *Princeton Univ. Press, Princeton, NJ [ua]* (2008).
- [18] Philipp Jorkowski and Rolf Schuhmann. “Higher-order sensitivity analysis of periodic 3-D eigenvalue problems for electromagnetic field calculations”. In: *Advances in Radio Science* 15 (2017), pp. 215–221.

- [19] Philipp Jorkowski and Rolf Schuhmann. “Mode tracking for parametrized eigenvalue problems in computational electromagnetics”. In: *2018 International Applied Computational Electromagnetics Society Symposium (ACES)*. IEEE, 2018, pp. 1–2.
- [20] Tosio Kato. *Perturbation theory for linear operators*. Vol. 132. Springer Science & Business Media, 2013.
- [21] Ludger Kaup and Burchard Kaup. *Holomorphic functions of several variables: an introduction to the fundamental theory*. Vol. 3. Walter de Gruyter, 2011.
- [22] Dirk Klindworth and Kersten Schmidt. “An efficient calculation of photonic crystal band structures using Taylor expansions”. In: *Communications in Computational Physics* 16.5 (2014), pp. 1355–1388.
- [23] Peter A Kuchment. *Floquet theory for partial differential equations*. Vol. 60. Springer Science & Business Media, 1993.
- [24] D Labilloy et al. “Demonstration of cavity mode between two-dimensional photonic-crystal mirrors”. In: *Electronics Letters* 33.23 (1997), pp. 1978–1980.
- [25] Florian Maurin et al. “Probability that a band-gap extremum is located on the irreducible Brillouin-zone contour for the 17 different plane crystallographic lattices”. In: *International Journal of Solids and Structures* 135 (2018), pp. 26–36.
- [26] Nicholas J Rose. “Linear algebra and its applications (gilbert strang)”. In: *SIAM Review* 24.4 (1982), pp. 499–501.
- [27] Philip Russell. “Photonic crystal fibers”. In: *science* 299.5605 (2003), pp. 358–362.
- [28] Herbert E Salzer. “Lagrangian interpolation at the Chebyshev points x_n , $\nu \equiv \cos(\nu\pi/n)$, $\nu = 0(1)n$; some unnoted advantages”. In: *The Computer Journal* 15.2 (1972), pp. 156–159.
- [29] Stefan A Sauter and Christoph Schwab. “Boundary element methods”. In: *Boundary Element Methods*. Springer, 2010, pp. 183–287.
- [30] Christian Scheiber et al. “A model order reduction method for efficient band structure calculations of photonic crystals”. In: *IEEE transactions on magnetics* 47.5 (2011), pp. 1534–1537.
- [31] Kersten Schmidt and Peter Kauf. “Computation of the band structure of two-dimensional photonic crystals with hp finite elements”. In: *Computer Methods in Applied Mechanics and Engineering* 198.13-14 (2009), pp. 1249–1259.
- [32] Mark A Taylor, Beth A Wingate, and Rachel E Vincent. “An algorithm for computing Fekete points in the triangle”. In: *SIAM Journal on Numerical Analysis* 38.5 (2000), pp. 1707–1720.
- [33] Lloyd N Trefethen. *Approximation Theory and Approximation Practice, Extended Edition*. SIAM, 2019.
- [34] Calvin H Wilcox. *Theory of Bloch Waves*. Tech. rep. UTAH UNIV SALT LAKE CITY DEPT OF MATHEMATICS, 1977.
- [35] Mehmet Fatih Yanik et al. “All-optical transistor action with bistable switching in a photonic crystal cross-waveguide geometry”. In: *Optics letters* 28.24 (2003), pp. 2506–2508.